

# Properties of vertically self-gravitating accretion discs with a dissipative corona

Fazeleh Khajenabi<sup>1\*</sup> and Peter Duffy<sup>1†</sup>

<sup>1</sup>*School of Physics, University College Dublin, Belfield, Dublin 4, Ireland*

31 October 2018

## ABSTRACT

The steady-state structure of a disc with a corona is analyzed when the vertical component of the gravitational force due to the self-gravity of the disc is considered. For the energy exchange between the disc and the corona, we assume a fraction  $f$  of the dissipated energy inside the accretion disc is transported to the corona via the magnetic tubes. Analytical solutions corresponding to a prescription for  $f$  (in which this parameter directly depends on the ratio of the gas pressure to the total pressure) or free  $f$  are presented and their physical properties are studied in detail. We show that the existence of the corona not only decreases the temperature of the disc, but also increases the surface density. The vertical component of the gravitational force due to the self-gravity of the disc decreases the self-gravitating radius and the mass of the fragments at this radius. However, as more energy is transported from the disc to the corona, the effect of the vertical component of the gravitational force due to the self-gravity of the disc on the self-gravitating radius becomes weaker, though the mass of the fragments is reduced irrespective of the amount of the energy exchange from the disc to the corona.

**Key words:** galaxies: active - black hole: physics - accretion discs

## 1 INTRODUCTION

Accretion plays a crucial role in the processes of energy liberation and mass accumulation near the cores of compact astronomical objects (Bertout 1989; Robinson 1976; Hunter, Ball & Gottesmanet 1984; Kohler 1995), and in particular for Active Galactic Nuclei (AGN) (Shields 1978 ;Osterbrock 1993;Szuszkiewicz 2001; Czerny 2007). Self-gravity has global consequences on the disc shape, influencing the location of its inner and outer edges, as well as the disc geometrical thickness (Karas, Huré & Semerák 2004). The role of self-gravity has been separated into that from its vertical component (e.g., Fukue & Sakamoto 1992; Huré 1998) or from its radial component (Lu, Yang & Wu 1997), and from combination of two (Yang & Liu 1990; Bertin & Lodato 1999). The vertical structure of accretion discs of galactic nuclei is affected by their own self-gravity and the gravitational force of the central object, especially in the middle and outer regions, where the vertical component of the disc gravitational field exceeds the corresponding vertical component due to the central object.

In addition to the role of self-gravity, one of the main open issues in the physics of black hole accretion discs is the relationship between the disc MRI-driven turbulent viscosity and the generation of a hot corona, which is postulated in order to explain the observed X-ray emission (Liang & Price 1977; Galeev, Rosner & Vaiana 1979; Blackman & Field 2000; Kuncic & Bicknell 2004). Furthermore, theoretical simulations successfully reproduce the observed spectra by assuming a certain fraction of gravitational energy is released as hot gas (e.g., Haardt& Maraschi 1991; Svensson & Zdziarski 1994; Kawaguchi, Shimura & Minishige 2001) and/or a certain spatial distribution of the hot gas (e.g., Merloni & Fabian 2001b). Svensson & Zdziarski (1994) studied a disc-corona system, in which a major fraction of the power released when the cold matter accretes is transported to and dissipated in the corona. They showed that the steady-state structure of the disc significantly modified due to the existence of a corona. Miller & Stone (2000) showed that the primary saturation mechanism of the MRI is local dissipation, about twenty five percent of magnetic energy generated by MRI within two scale heights escapes because of buoyancy, producing a strongly magnetized corona above the disc. It was shown by Merloni & Fabian (2001a) that the inferred thermal energy content of the corona, in all black hole systems, is far too low to explain their observed hard

\* E-mail: fazeleh.khajenabi@ucd.ie (FK);

† E-mail: peter.duffy@ucd.ie (PD)

X-ray luminosities, unless either the size of the corona is at least of the order of  $10^3$  Schwarzschild radii, or the corona itself is in fact a reservoir, where the energy is mainly stored in the form of a magnetic field generated by a sheared rotator.

Following these considerations Khajenabi & Shadmehri (2007) (hereafter KS) studied the gravitational instability of an accretion disc with a corona. They showed that the disc becomes more gravitationally unstable due to the existence of the corona. Because of the corona, not only does the self-gravitating radius decrease, but also the mass of the fragments at this radius increases (KS). However, KS did not take into account the vertical component of the gravitational force due to the self-gravity of the disc. Also, their analysis was based just on the Toomre parameter criteria. Actually, theory and simulations (Gammie 2001; Rice et al. 2003, 2005; Lodato & Rice 2004; Mejia et al. 2005) show that *two* conditions should be fulfilled for accretion discs to fragment gravitationally. First, the accretion disc must be massive enough so that gravity can overcome thermal pressure and centrifugal support, which implies a value of less than unity for the Toomre parameter (Toomre 1964). Second, the disc must cool fast enough for the compressional energy provided by the collapse to be radiated away. So, according to the numerical simulations (Gammie 2001; Rice et al. 2003, 2005; Lodato & Rice 2004; Mejia et al. 2005), the cooling time-scale must be of the order of the dynamical time-scale. For an accretion disc with a corona, we believed that the corona provides another mechanism for the cooling of the disc and so, existence of the corona decreases the cooling time-scale.

In this paper, we extend the analysis of KS in different directions: (i) Toomre parameter and the cooling time-scale conditions are considered as criteria for the fragmentation of the disc; (ii) the vertical component of the gravitational force due to the self-gravity of the disc is considered; (iii) for the fraction of the dissipated energy inside the disc that is transported to the corona, we consider two cases. In the first case, this fraction depends on the physical variables of the system (Merloni & Nayakshin 2006); and in the other case, this fraction is assumed to be constant and we consider it as a free parameter of the model. In the next section, the basic assumptions and the equations are presented. We analyse properties of the solutions in Section 3. The gravitational stability of our solutions is studied in detail in Section 4. By studying the gravitational stability of such a system, we address the effect of self-gravity on disc stability and fragmentation. We conclude with a summary of the results and a discussion in the final section.

## 2 GENERAL FORMULATION

As a result of differential rotation the gas is heated, loses angular momentum and a slow (subsonic) radial drift results. In a steady state the mass accretion rate is constant, and the local viscous energy release is balanced by the radiative cooling. In the direction perpendicular to the plane of the disc, hydrostatic equilibrium is assumed. The rotation curve is dominated by a Newtonian point mass  $M$ , as relativistic effects are only important at small radii. Thus, the rotational

angular velocity of the disc is approximately Keplerian, i.e.  $\Omega_K = \sqrt{GM/R^3}$ . Although we neglect the radial component of the self-gravity of the disc, the self-gravity of the disc in the vertical direction that modifies the hydrostatic equilibrium of the disc is included in our model. We take it into account with the extra assumption that the accretion disc is homogeneous and extends to infinity, as done in several other models (Paczynski 1978; Kozłowski, Wiita & Paczynski 1979; Sakimoto & Coroniti 1981; Shore & White 1982; Cannizzo & Reiff 1992; Hure et al. 1994a). The weight of the corona is negligible as has been shown by Svensson & Zdziarski (1994). So, the vertical hydrostatic equilibrium of the disc implies

$$\frac{p}{\Sigma} = \frac{\Omega_K^2 H}{2} \left(1 + \frac{4\pi G \rho}{\Omega_K^2}\right), \quad (1)$$

where we introduce

$$\zeta = \frac{4\pi G \rho}{\Omega_K^2}, \quad (2)$$

which measures, along the axis of rotation, the acceleration due to self-gravity as a fraction of the central gravitational acceleration. With this definition, equation (1) can be rewritten as

$$\frac{p}{\Sigma} = \frac{\Omega_K^2 H}{2} (1 + \zeta). \quad (3)$$

In what follows, when we discuss solutions without self-gravity of the disc, we mean solutions that are obtained by neglecting  $\zeta$  in the above equation (see KS). Also, by solutions with self-gravity of the disc, we mean solutions that are obtained by considering  $\zeta$  in the above equation. We obtain solutions with self-gravity in this paper and illustrate the possible effect of the self-gravity by making comparisons to solutions without self-gravity.

The basic remaining equations of our model are similar to KS. However, we briefly mention the equations and basic assumptions for completeness. We consider a more general prescription for the viscous stresses  $\tau_{r\phi}$  (Taam & Lin 1984; Watarai & Mineshige 2003; Merloni & Nayakshin 2006):

$$\tau_{r\phi} = -\alpha_0 p^{1-\mu/2} p_{\text{gas}}^{\mu/2}, \quad (4)$$

where  $\alpha_0$  and  $0 \leq \mu \leq 2$  are constants and  $p$  is the sum of the gas and radiation pressures. Phenomenological models generally assume that at each radius, a fraction  $f$  of the accretion energy is released in the reconnected magnetic corona. Assuming that in MRI-turbulence discs such a fraction  $f$  of the binding energy is transported from large to small depths by Poynting flux, Merloni & Nayakshin (2006) estimated the fraction  $f$  as

$$f = \sqrt{2\alpha_0 \beta^{\mu/2}}, \quad (5)$$

where  $\beta$  is the ratio of gas pressure to the total pressure (The MN prescription hereafter). With expressions (4) and (5) for the viscous stresses and dissipated power respectively, we can construct the basic equations describing the disc. The azimuthal component of the equation of motion gives

$$8\pi\alpha_0 H (p_{\text{gas}})^{\mu/2} p^{(2-\mu)/2} = 3\Omega_K \dot{M} J(R), \quad (6)$$

where  $J(R) = 1 - \sqrt{R_{\text{in}}/R}$  and  $R_{\text{in}}$  denotes the inner boundary of disc. Since we are interested in the regions of the disc

with radii much larger than  $R_{\text{in}}$ , we have  $J \approx 1$ , but we keep the more general expression in what follows. Energy conservation implies that

$$\sigma T_{\text{eff}}^4 = \frac{3}{8\pi} \Omega_K^2 \dot{M} J(R) (1-f). \quad (7)$$

Finally, with the vertical transport of heat dominated by radiative diffusion we have a relation between the midplane and surface temperatures given by

$$T = \left(\frac{3}{8} \kappa \Sigma\right)^{1/4} T_{\text{eff}}, \quad (8)$$

where  $\kappa$  is the opacity coefficient.

Equations (3), (6), (7) and (8) enable us to find  $p$  and  $T$  and  $\rho$  as functions of  $R$  with  $\beta$  and  $\zeta$  the critical input parameters. Thus,

$$T = \left(\frac{4\sigma\Omega_K}{3\kappa\alpha_0}\right)^{-1/2} \left(\frac{16\pi^2\alpha_0^2 ck_B}{3\sigma\mu_m m_H \dot{M}^2 \Omega_K^4 J^2}\right)^{-1/3} \frac{1}{(1+\zeta)^{1/6}} \times \frac{(1-\sqrt{2\alpha_0\beta^{\mu/2}})^{1/2}}{(1-\beta)^{1/3}} \beta^{(4-\mu)/12}, \quad (9)$$

$$p = \left(\frac{4\sigma\Omega_K}{3\kappa\alpha_0}\right)^{-1/2} \left(\frac{16\pi^2\alpha_0^2 ck_B}{3\sigma\mu_m m_H \dot{M}^2 \Omega_K^4 J^2}\right)^{-2/3} (1+\zeta)^{1/6} \times \frac{(1-\sqrt{2\alpha_0\beta^{\mu/2}})^{1/2}}{(1-\beta)^{2/3}} \beta^{(8-5\mu)/12}. \quad (10)$$

$$\rho = \left(\frac{8\pi\alpha_0}{3\Omega_K^2 \dot{M} J}\right)^2 \frac{p^3}{(1+\zeta)} \beta^\mu.$$

There are two algebraic equations for  $\beta$  and  $\zeta$  as follows

$$\frac{k_B}{\mu_m m_H} \left(\frac{4\sigma\Omega_K}{3\kappa\alpha_0}\right)^{-3/2} \left(\frac{8\pi\alpha_0}{3\Omega_K^2 \dot{M} J}\right)^2 \left(\frac{16\pi^2\alpha_0^2 ck_B}{3\sigma\mu_m m_H \dot{M}^2 \Omega_K^4 J^2}\right)^{-5/3} \times (1+\zeta)^{-5/6} \frac{(1-\sqrt{2\alpha_0\beta^{\mu/2}})^{3/2}}{(1-\beta)^{5/3}} \beta^{(8+\mu)/12} = 1, \quad (11)$$

$$\zeta(1+\zeta)^{1/2} = \frac{4\pi G}{\Omega_K^2} \left(\frac{4\sigma\Omega_K}{3\kappa\alpha_0}\right)^{-3/2} \left(\frac{8\pi\alpha_0}{3\Omega_K^2 \dot{M} J}\right)^2 \times \left(\frac{16\pi^2\alpha_0^2 ck_B}{3\sigma\mu_m m_H \dot{M}^2 \Omega_K^4 J^2}\right)^{-2} \frac{(1-\sqrt{2\alpha_0\beta^{\mu/2}})^{3/2}}{(1-\beta)^2} \beta^{(8-\mu)/4}, \quad (12)$$

where  $\mu_m$  is the mean particle mass in units of the hydrogen atom mass,  $m_H$ . The other constants have their usual meaning. These two equations give us  $\zeta$  as follows

$$\zeta = \frac{4\pi G}{\Omega_K^2} \left(\frac{4\sigma\Omega_K}{3\kappa\alpha_0}\right)^{-3/5} \left(\frac{8\pi\alpha_0}{3\Omega_K^2 \dot{M} J}\right)^{4/5} \left(\frac{16\pi^2\alpha_0^2 ck_B}{3\sigma\mu_m m_H \dot{M}^2 \Omega_K^4 J^2}\right)^{-1} \times \left(\frac{k_B}{\mu m_H}\right)^{-3/5} (1-\sqrt{2\alpha_0\beta^{\mu/2}})^{3/5} \frac{\beta^{(16-3\mu)/10}}{(1-\beta)} \quad (13)$$

Now equation (13) enables us to find  $T$ ,  $P$  and  $\rho$  as functions of  $R$ ,  $\beta$  and the other input parameters in the form

$$T = \left(\frac{4\sigma\Omega_K}{3\kappa\alpha_0}\right)^{-1/5} \left(\frac{8\pi\alpha_0}{3\Omega_K^2 \dot{M} J}\right)^{-2/5} \left(\frac{k_B}{\mu m_H}\right)^{-1/5} \times (1-\sqrt{2\alpha_0\beta^{\mu/2}})^{1/5} \beta^{(2-\mu)/10}, \quad (14)$$

$$p = \left(\frac{4\sigma\Omega_K}{3\kappa\alpha_0}\right)^{-4/5} \left(\frac{8\pi\alpha_0}{3\Omega_K^2 \dot{M} J}\right)^{2/5} \left(\frac{k_B}{\mu m_H}\right)^{1/5}$$

$$\times \left(\frac{16\pi^2\alpha_0^2 ck_B}{3\sigma\mu_m m_H \dot{M}^2 \Omega_K^4 J^2}\right)^{-1} \frac{(1-\sqrt{2\alpha_0\beta^{\mu/2}})^{4/5}}{(1-\beta)} \beta^{(4-2\mu)/5}, \quad (15)$$

$$\rho = \left(\frac{4\sigma\Omega_K}{3\kappa\alpha_0}\right)^{-3/5} \left(\frac{8\pi\alpha_0}{3\Omega_K^2 \dot{M} J}\right)^{4/5} \left(\frac{k_B}{\mu m_H}\right)^{-3/5} \times \left(\frac{16\pi^2\alpha_0^2 ck_B}{3\sigma\mu_m m_H \dot{M}^2 \Omega_K^4 J^2}\right)^{-1} \frac{(1-\sqrt{2\alpha_0\beta^{\mu/2}})^{3/5}}{(1-\beta)} \beta^{(16-3\mu)/10}. \quad (16)$$

In order to study the behavior of our solutions, it is more convenient to introduce dimensionless variables. For the central mass  $M$ , we introduce  $M_8 = M/(10^8 M_\odot)$  and for the radial distance  $R$ , we have  $r_3 = R/(10^3 R_S)$ , where  $R_S = 2GM/c^2$  is the Schwarzschild radius. The mass accretion rate can be written as

$$\dot{M} = \frac{l_E}{\epsilon} \frac{4\pi GM}{\kappa_{e.s.} c} = \frac{l_E}{\epsilon} \frac{L_E}{c^2}, \quad (17)$$

where  $l_E = L/L_E$  is the dimensionless disc luminosity relative to the Eddington limit,  $\epsilon = L/(\dot{M}c^2)$  is the radiative efficiency and  $\kappa_{e.s.} \approx 0.04 \text{ m}^2\text{kg}^{-1}$  is the electron opacity. In our analysis, we will use the nondimensional factor  $l_E/\epsilon$  as a free parameter so that by changing this parameter we can consider appropriate values of the accretion rate. However, some authors introduce different forms for the accretion rate. For example, Nayakshin & Cuadra (2005) who studied gravitational stability of the Galactic Center, introduced  $\dot{M} = (\dot{m}/\epsilon)(L_E/c^2)$  with  $\epsilon \approx 0.06$  and  $\dot{m} = 0.03$  to 1. These values, which are appropriate for the Galactic Center, correspond to  $l_E/\epsilon \approx 0.5$  to 16.6 in our notation. Also, for a central mass with mass  $M = 10^8 M_\odot$ , Goodman & Tan (2004) proposed  $l_E/\epsilon = 10$ . Thus, in our analysis, the corresponding range of values for  $l_E/\epsilon$  is from 1 to 10.

Our solutions for  $T$ ,  $P$  and  $\rho$  become

$$T = 1.65 \times 10^4 \alpha_0^{-1/5} \hat{\kappa}^{1/5} M_8^{-1/5} \left(\frac{l_E}{\epsilon}\right)^{2/5} J^{2/5} r_3^{-9/10} \times \beta^{(2-\mu)/10} (1-\sqrt{2\alpha_0\beta^{\mu/2}})^{1/5}, \quad (18)$$

$$p = 18.72 \times \alpha_0^{-4/5} \hat{\kappa}^{4/5} M_8^{-4/5} \left(\frac{l_E}{\epsilon}\right)^{8/5} J^{8/5} r_3^{-18/5} \times \beta^{(4-2\mu)/5} (1-\beta)^{-1} (1-\sqrt{2\alpha_0\beta^{\mu/2}})^{4/5}, \quad (19)$$

$$\rho = 0.823 \times 10^{-7} \alpha_0^{-3/5} \hat{\kappa}^{3/5} M_8^{-3/5} \left(\frac{l_E}{\epsilon}\right)^{6/5} J^{6/5} r_3^{-27/10} \times \beta^{(16-3\mu)/10} (1-\beta)^{-1} (1-\sqrt{2\alpha_0\beta^{\mu/2}})^{3/5}, \quad (20)$$

$$\frac{H}{R} = 6.7 \times 10^{-3} \alpha_0^{-1/5} \hat{\kappa}^{-4/5} M_8^{-1/5} \left(\frac{l_E}{\epsilon}\right)^{-3/5} J^{-3/5} r_3^{11/10} \times \beta^{-(8+\mu)/10} (1-\beta) (1-\sqrt{2\alpha_0\beta^{\mu/2}})^{-4/5}, \quad (21)$$

We can also calculate the surface density as

$$\Sigma = 3.292 \times 10^5 \alpha_0^{-4/5} \hat{\kappa}^{-1/5} M_8^{1/5} \left(\frac{l_E}{\epsilon}\right)^{3/5} J^{3/5} r_3^{-3/5} \times \beta^{(4-2\mu)/5} (1-\sqrt{2\alpha_0\beta^{\mu/2}})^{-1/5}. \quad (22)$$

and the ratio  $\beta$  is obtained from nondimensional form of equations (11) and (13), i.e.

$$\zeta = 0.134 \times \alpha_0^{-3/5} \hat{\kappa}^{3/5} M_8^{7/5} \left(\frac{l_E}{\epsilon}\right)^{6/5} J^{6/5} r_3^{3/10} \times \beta^{(16-3\mu)/10} (1-\beta)^{-1} (1-\sqrt{2\alpha_0\beta^{\mu/2}})^{3/5} \quad (23)$$

$$0.216 \times \alpha_0^{1/5} \hat{\kappa}^{9/5} M_8^{1/5} \left(\frac{l_E}{\epsilon}\right)^{8/5} J^{8/5} r_3^{-21/10} \\ \times \beta^{(8+\mu)/10} (1-\beta)^{-2} (1 - \sqrt{2\alpha_0\beta^{\mu/2}})^{9/5} - 1 - \zeta = 0 \quad (24)$$

where  $\hat{\kappa} = \kappa/\kappa_{e.s.}$  and we assumed  $\mu_m = 0.6$ .

Equations (18), (19), (20) and (21) describe the structure of a self-gravitating disc with a dissipative corona. However, the physical variables depend not only on the radial distance but also on  $\beta$  and  $\zeta$  which can be calculated at each radius from algebraic equations (23) and (24). In the next section we will analyze our solution, in particular the gravitational stability of the disc.

### 3 ANALYSIS

We can solve algebraic equations (23) and (24) numerically at each radius to obtain the ratios  $\beta$  and  $\zeta$ . Having these parameters, physical variables are obtained based on our analytical solutions. Since we are interested in gravitational stability of the disc, we can approximate  $J(R) \simeq 1$  for  $R \gg R_{in}$ . Also we fix the central mass  $M_8 = 1$ , the opacity  $\hat{\kappa} = 1$  and the viscosity exponent  $\mu = 1$ , but vary the other input parameters. However, for the transport of energy from the disc to the corona (i.e. the fraction  $f$  in our approach), we may either consider the MN prescription (in which  $f$  is not constant) or assume that the fraction  $f$  is constant and use it as a free parameter of the model. We study properties of the solutions in both cases in the next two subsections. Interestingly, typical behaviors of the solutions are similar qualitatively, though precise values of the physical variables at each radius depend on the mathematical prescription of the fraction  $f$ . The possible effects of the self-gravity of the disc in both forms of prescription for the fraction  $f$  are illustrated by appropriate plots in the next subsections.

#### 3.1 Properties of the solutions corresponding to

$$f = \sqrt{2\alpha_0\beta^{\mu/2}}$$

##### 3.1.1 General properties

Figure 1 shows the typical behaviours of the solutions for discs with (dashed curves) and without (solid curves) a corona. Each curve is labeled by the appropriate values of  $(\alpha_0, l_E/\epsilon)$ . Behavior of the surface density is shown in the top left-hand plot of Figure 1. For the same input parameters, the presence of a corona enhances the surface density, and the surface density generally displays two regimes in the inner and outer regions. The size of the inner part is sensitive to the values of the input parameters. For a fixed viscosity coefficient, when the accretion rate increases the surface density in the inner part decreases, while the surface density at the outer parts increases in both cases with and without a corona. For a fixed accretion rate when the viscosity coefficient increases, the surface density decreases. Generally, we see that the corona becomes more effective when the viscosity and the accretion rate have larger values. Finally, at large radii the surface density is in proportion to  $R^{-0.6}$ .

The top right-hand plot of Figure 1 shows the ratio of disc thickness to the radius. The corona causes the disc to

become thinner in comparison with the same disc without a corona. In the absence of a corona, for a fixed rate of accretion, viscosity increases the disc thickness. However, in a disc with a corona, so long as the accretion rate is constant, the thickness of the disc decreases in the inner part and increases in the outer part due to increase of the viscosity coefficient. With a fixed viscosity coefficient and increased accretion rate, the thickness of the disc increases in the inner part, but the thickness of the outer part decreases in both the case of a disc with a corona and the case without a corona. The disc thickness scales like  $R^{-1.3}$  at large radii.

The bottom left-hand plot of Figure 1 shows that the presence of a corona serves to cool the disc because of the energy transported from the disc to the corona. Generally, for a fixed accretion rate when the viscosity coefficient increases, the disc temperature decreases because more energy is transported from the disc to the corona. But for a fixed viscosity coefficient when the accretion rate increases, then the temperature of the disc increases too. At large radii the temperature is changing in proportion to  $R^{-0.9}$ .

The bottom right-hand plot of Figure 1 shows that the corona causes the disc to become more self-gravitating in the vertical direction in comparison with the case without a corona while, for a fixed accretion rate, when the viscosity coefficient increases, the self-gravity of the disc in the vertical direction decreases. However, for a fixed viscosity coefficient, when the accretion rate increases, there are two regimes, in both the case with and without a corona. At smaller radii, self-gravity of the disc in the vertical direction decreases, but as we go to the larger radii the vertical component of self-gravity becomes more significant. At larger radii the ratio  $\zeta$  varies in proportion to  $R^{2.75}$ . This plot shows that the vertical component of the self-gravity can be comparable to the vertical component of the gravitational force of the central object at radii that are not large. Clearly, this radius is within a distance from the central object where the corona can exist. For instance for a pair (0.03, 1), the self-gravity of the disc is of the order of the gravitational force of the central mass at around  $R \sim 300R_s$ . For the (0.03, 10) case this happens at around  $R \sim 400R_s$ . It clearly shows that self-gravity in the vertical direction is important for a disc-corona system even at not large radii from the central object where a corona exists.

##### 3.1.2 The effect of the self-gravity of the disc

We study the possible effects of the self-gravity of the disc on the profiles of the physical variables of the disc in this subsection. Gravitational stability of the disc and the role of the self-gravity is studied in Section 4 separately. Figure 2 compares profiles of the solutions with self-gravity with those without self-gravity (KS solutions). The input parameters are similar to Figure 1 and each curve is labeled by a pair  $(\alpha_0, l_E/\epsilon)$ . We see that the surface density at radii smaller than  $10^3$  Schwarzschild radius decreases due to the effect of self-gravity of the disc, irrespective of the viscosity coefficient and the accretion rate. Although the fraction of  $\zeta$  is not very large at these radii, the profile of the surface density changes significantly because of the self-gravity of the disc.

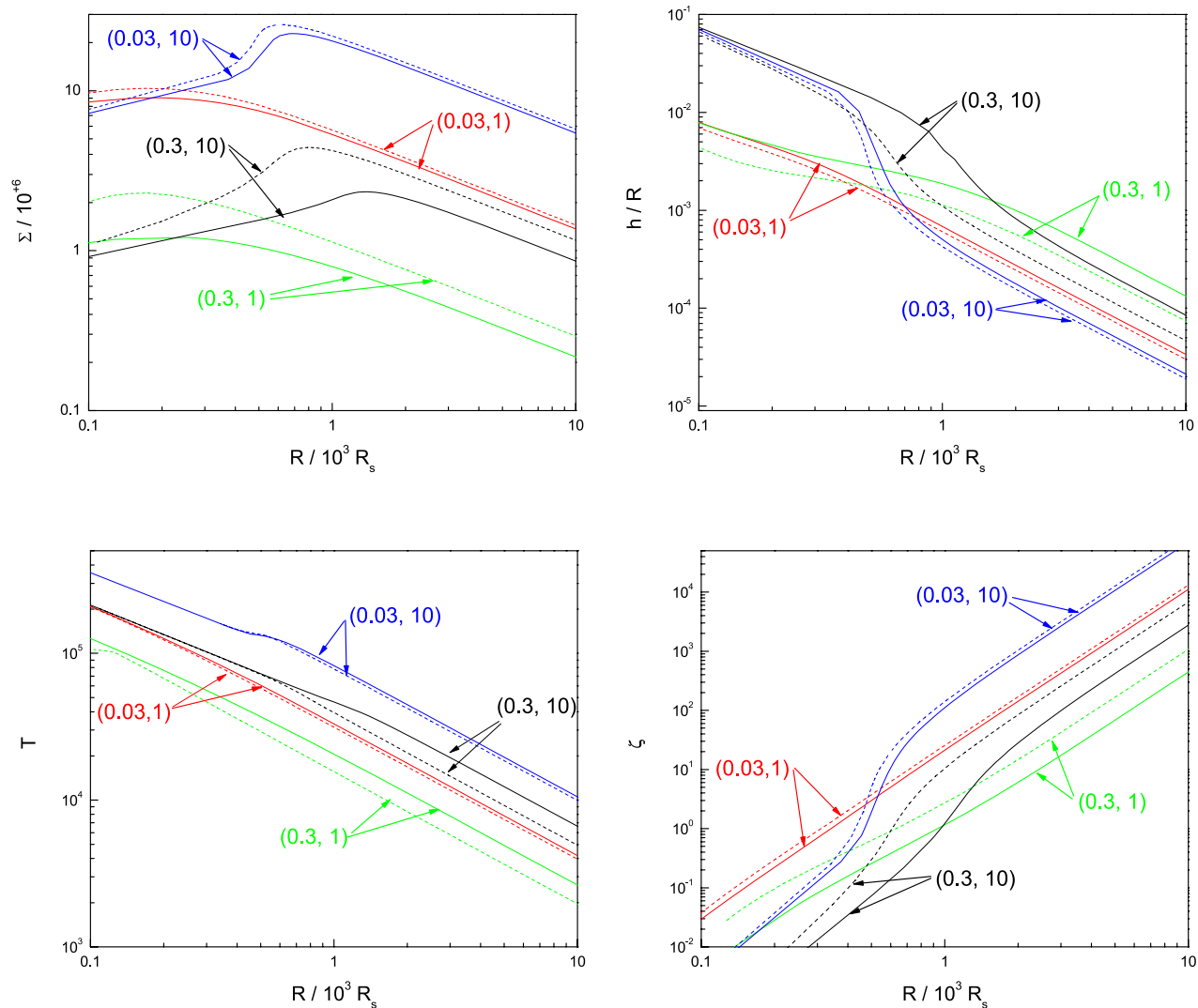


**Figure 1.** Profiles of the physical variables for a disc without a corona (*solid lines*) and with a corona (*dashed lines*) vs. radial location in the disc with  $\mu = 1.0$ ,  $\mu_m = 0.6$ ,  $k = 1$  and  $M_s = 1$ . Each curve is labeled by the viscosity coefficient  $\alpha_0$  and the accretion rate  $l_E/\epsilon$  as a pair  $(\alpha_0, l_E/\epsilon)$ . A different color is used for the curve corresponding to each pair of the input parameters. Here, the MN prescription for the dissipated energy into the corona has been considered. Since the amount of energy transported into the corona increases with the viscosity coefficient, the possible effects of the corona on the profiles are more evident for the higher viscosity coefficient. While the temperature of the disc decreases because of the corona, the surface density of the disc increases.

Also, the self-gravity of the disc implies a thinner disc with a smaller opening angle. This reduction in the thickness of the disc is at all radii and for all the input parameters. In our analysis, we do not consider the vertical structure of the accretion disc. But in studies of the vertical structure of the accretion discs and analysis of the energy transport in this direction (e.g., via convection), one should note that the self-gravity of the disc significantly reduces the thickness of the disc according to our analytical solutions for a disc

and corona system. However, the temperature of the disc is independent of the self-gravity of the disc for all the input parameters. However, the ratio of the gas pressure to the total pressure, in particular for high accretion rates, increases because of the self-gravity of the disc.

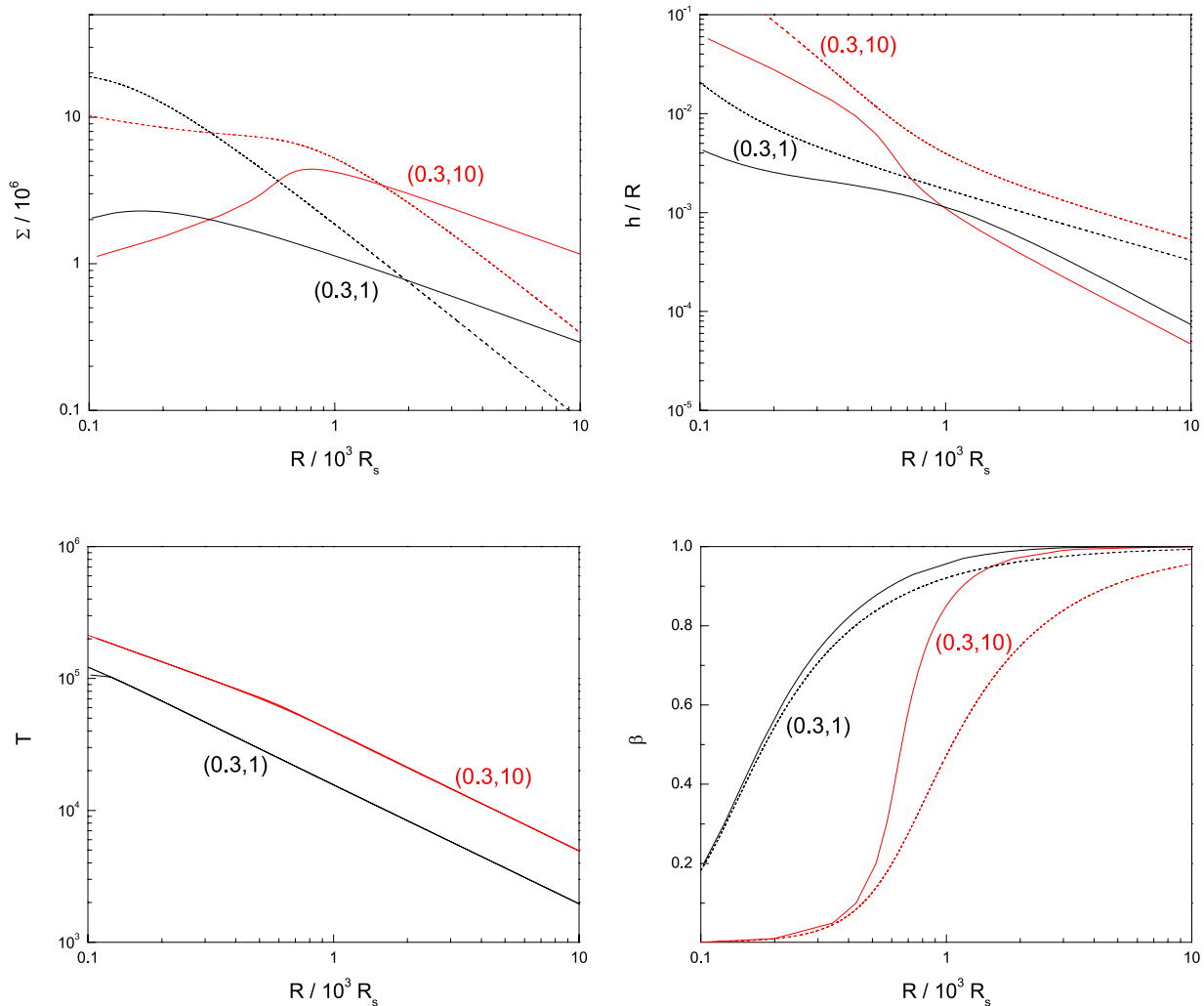


**Figure 2.** Effects of the self-gravity of the disc on the profiles of the physical variables are shown in these plots by comparing our solutions with a corona (*solid lines*) and those solutions with a corona but neglecting the vertical component of the self-gravity of the disc (KS solutions, *dashed lines*). The input parameters are the same as Figure 1. Each curve is labeled by a pair of input parameters. Different colors are used to denote the curves corresponding to the different pair of input parameters. Here, the MN prescription for the dissipated energy into the corona has been considered. We see reduction in the surface density of the disc at radii approximately smaller than  $10^3 R_s$  due to the self-gravity of the disc. Beyond this radius the surface density increases because of the self-gravity of the disc. However, the temperature of the disc is independent of the self-gravity of the disc.

### 3.2 Properties of the solutions when $f$ is a free parameter

Svensson & Zdziarski (1994) presented analytical solutions for the disc-corona systems, in which a constant fraction  $f$  is dissipated into the corona. Now, we analysis properties of the physical variables of those solutions that correspond to a constant fraction  $f$ . Figure 3 shows profiles for  $\mu = 1.0$ ,  $\mu_m = 0.6$ ,  $\hat{k} = 1$ ,  $\alpha_0 = 0.3$ ,  $l_E/\epsilon = 1$  and  $M_8 = 1$ . Each curve

is labeled by the fraction  $f$ , which is assumed to be constant. For easier comparison, solutions without self-gravity are shown by dashed lines. Interestingly, properties of the solutions are qualitatively similar to the solutions with the MN prescription. Here, the surface density of the disc decreases due to the self-gravity of the disc at radii smaller than  $10^3$  Schwarzschild radius. This reduction is independent of the amount of the energy transported to the corona.

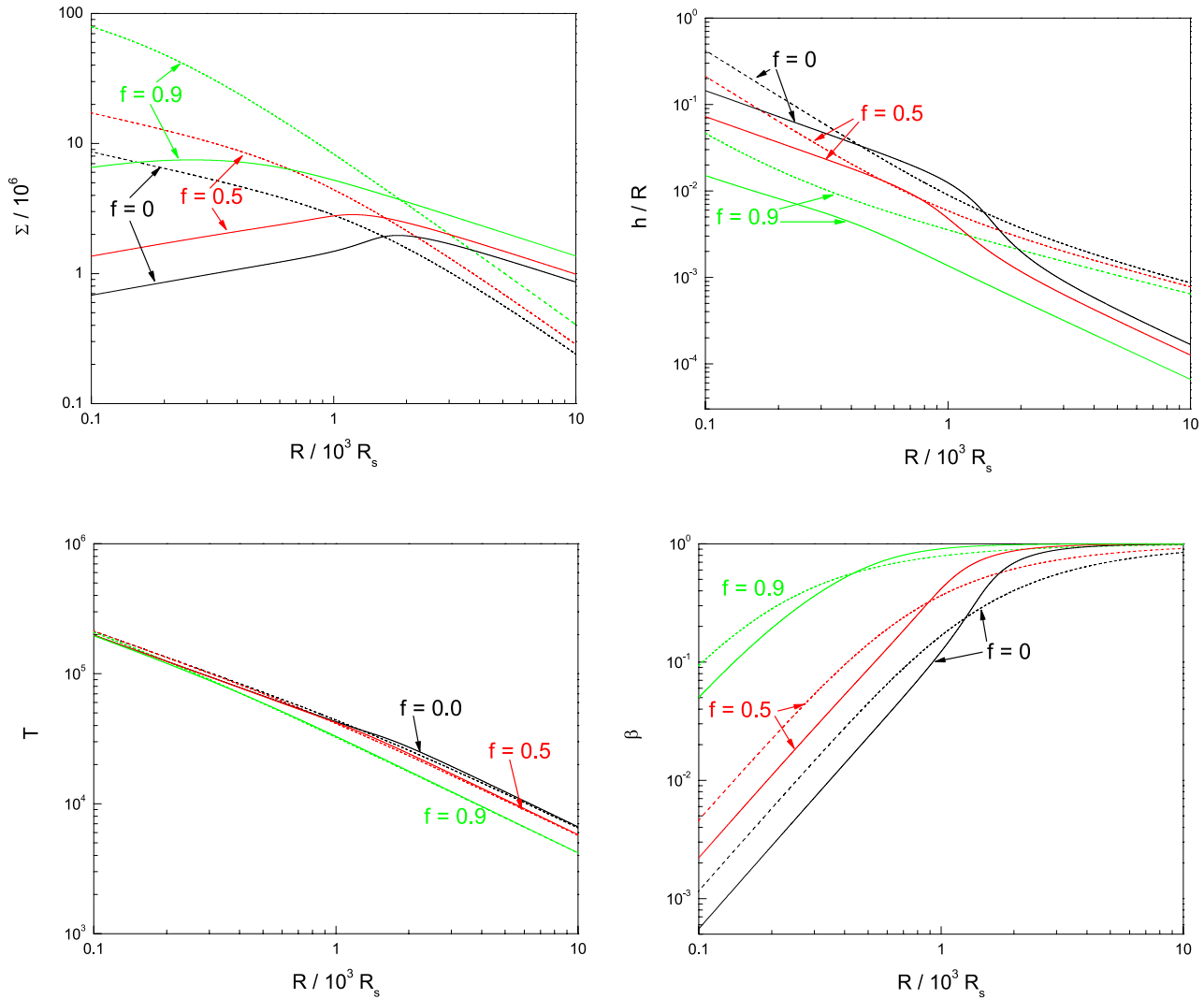


**Figure 3.** Physical profiles of the disc when the fraction of dissipated energy into the corona is constant. The input parameters are  $\mu = 1.0$ ,  $\mu_m = 0.6$ ,  $k = 1$ ,  $\alpha_0 = 0.3$ ,  $l_E/\epsilon = 10$  and  $M_S = 1$ . Each curve is labeled by the fraction  $f$  (which is assumed to be constant) and is shown by different color. *Solid lines* are for the solutions with the vertical component of the self-gravity of the disc and the *dashed lines* show solutions when self-gravity of the disc is neglected. These curves are showing similar behaviors to when the fraction  $f$  is described by the MN prescription (Figures 1 and 2). Existence of the corona lead to an increase of the surface density and a cooler disc. Also, the surface density in the inner parts of the disc reduces because of the vertical component of the self-gravity of the disc, though the surface density increases beyond these regions.

However, as the fraction  $f$  increases, the profile of the surface density shifts upward either with or without self-gravity of the disc. This means that as more energy is transported via magnetic tubes from the disc to the corona, the surface density increases.

The thickness of the disc also depends on the self-gravity of the disc and the fraction  $f$ . The disc becomes thinner when more energy is transferred from the disc to the

corona. Also, for a given fraction  $f$ , self-gravity of the disc causes the thickness of the disc to decrease. The thickness of the disc corresponding to the solutions with self-gravity is more sensitive to the fraction  $f$  compared with the solutions without self-gravity. Again, in this case, the existence of the corona implies a cooler disc, but the temperature of the disc is independent of the self-gravity of the disc. The ratio  $\beta$  also decreases at the inner parts of the disc due to

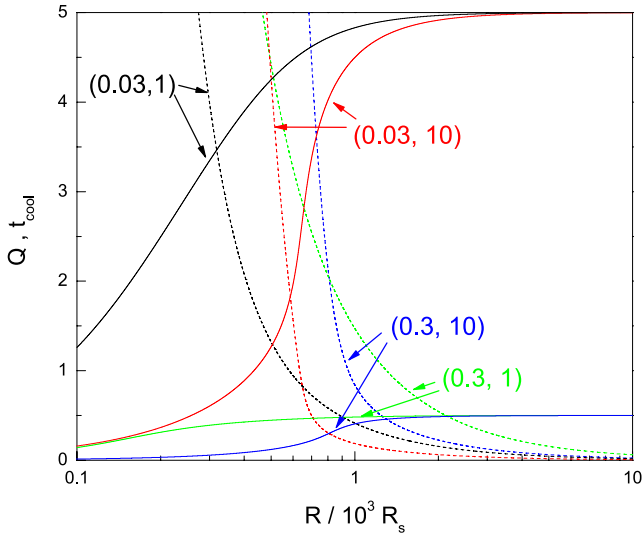


**Figure 4.** Profiles of the cooling time-scale  $t_{\text{cool}}$  (solid lines) and the Toomre parameter  $Q$  (dashed lines) vs. radial location in the disc. The curves are corresponding to the MN prescription and the input parameters are  $\mu = 1.0$ ,  $\mu_m = 0.6$ ,  $k = 1$ ,  $\gamma = 2$  and  $M_8 = 1$ . Each curve is labeled by a pair  $(\alpha_0, l_E/\epsilon)$  and is showing by a color.

the self-gravity of the disc. However, this reduction is more evident for a smaller fraction  $f$ .

#### 4 GRAVITATIONAL STABILITY OF THE DISC-CORONA SYSTEM

Having our analytical solutions for the steady-state structure of an accretion disc with a corona, we can study the gravitational stability of such a system. Although most authors have been using the Toomre parameter as the main criterion in order to address the gravitational stability of accretion discs (e.g., Goodman 2003; Goodman & Tan 2004; Nayakshin & Cuadra 2005), recent numerical simulations and physical considerations show that the cooling time-scale is another important physical factor (e.g., Gammie 2001; Lodato & Rice 2004). Also, the analysis of KS of the gravitational stability of an accretion disc with corona is based on just the Toomre parameter (they had also neglected self-gravity of the disc). In this subsection, we study gravitational stability of our solutions considering the Toomre pa-

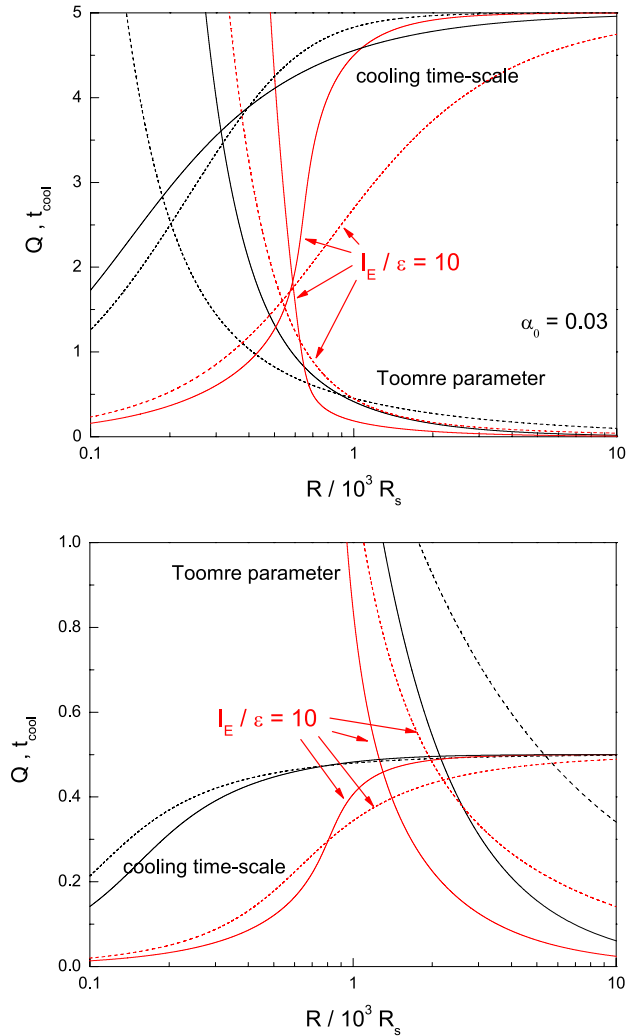


**Figure 5.** Profiles of the cooling time-scale  $t_{\text{cool}}$  and the Toomre parameter  $Q$  vs. radial location in the disc for  $\alpha_0 = 0.03$  (top) and  $\alpha_0 = 0.3$  (bottom). Solid curves are corresponding to our solutions, but dashed lines are for solutions neglecting self-gravity of the disc (KS solutions). The curves are corresponding to the MN prescription and the input parameters are  $\mu = 1.0$ ,  $\mu_m = 0.6$ ,  $k = 1$ ,  $\gamma = 2$  and  $M_8 = 1$ . Curves corresponding to  $l_E/\epsilon = 10$  are marked and the rest of the curves are for  $l_E/\epsilon = 1$ .

rameter and the cooling time-scale. Since solutions with free  $f$  and the MN prescription show qualitatively similar behaviors, the stability analysis is restricted to those corresponding to the solutions with the MN prescription. First, we calculate these parameters, then we do a parameter study.

##### 4.1 Toomre Parameter

It was shown by Toomre (1964) that a rotating disc is subject to gravitational instabilities when the  $Q$  parameter



$$Q = \frac{c_s \Omega}{\pi G \Sigma}, \quad (25)$$

becomes smaller than a critical value, which is close to unity, where  $c_s$  is the sound speed inside the accretion disc and  $\Omega = \Omega_K$  is the angular velocity. Having our analytical solution for the system, Toomre parameter of the model becomes

$$Q = 4.945 \times \alpha_0^{7/10} \hat{\kappa}^{3/10} M_8^{-13/10} \left(\frac{l_E}{\epsilon}\right)^{-2/5} J^{-2/5} r_3^{-27/20} \times \beta^{(7\mu-24)/20} (1 - \sqrt{2\alpha_0\beta^{\mu/2}})^{3/10}. \quad (26)$$

This equation along with two algebraic equations (23) and (24) give  $Q$  as a function of the radial distance. Generally,  $Q$  is much greater than unity in the inner parts of the disc which implies these regions are gravitationally stable and do not fragment. But the Toomre parameter decreases with increasing radial distance so that  $Q$  reaches the critical value of unity at a self-gravitating radius which we denote it by  $R_{\text{sg}}$ . Thus, all regions with  $R > R_{\text{sg}}$  are gravitationally unstable and may fragment. However, this is only true as long as the cooling time-scale also satisfies a criterion which will be explored in the next subsection.

It can be shown that when the Toomre parameter is of order unity the ratio  $\zeta$  is around 4.8 in our model. With  $Q = 1$ , we have

$$4\pi G \rho = \frac{2c_s \Omega_k}{H}. \quad (27)$$

When combined with equation (2) this gives

$$\zeta = \frac{2c_s}{H\Omega_k}. \quad (28)$$

From (3) and  $c_s = \sqrt{p/\rho}$ , we have

$$\frac{c_s}{H\Omega_k} = \sqrt{1 + \zeta}. \quad (29)$$

Using equations (28) and (29), we obtain an algebraic quadratic equation for  $\zeta$ . The only physical root of this equation is  $\zeta = 2(1 + \sqrt{2}) \simeq 4.8$ . This means that at a radius where the Toomre parameters is around unity, we have  $\zeta \simeq 4.8$ , i.e., the force of the self-gravity of the disc in the vertical direction is 4.8 times the vertical component of the gravitational force of the central object.

The most unstable wavelength for the  $Q \sim 1$  disc is of the order of the disc vertical scale height  $H$  (Toomre 1964). Thus, the most unstable mode has radial wave number  $k_{\text{mu}} = (QH)^{-1}$  and so the mass of a fragment at  $R = R_{\text{sg}}$  becomes

$$M_{\text{frag}} \approx \Sigma \left(\frac{2\pi}{k_{\text{mu}}}\right)^2 = 4\pi^2 \Sigma H^2, \quad (30)$$

which gives

$$M_{\text{frag}} = 0.126 \times 10^{34} \alpha_0^{1/5} \hat{\kappa}^{-6/5} M_8^{-4/5} \left(\frac{l_E}{\epsilon}\right)^{-7/5} J^{-7/5} r_3^{-6/5} \times \beta^{(\mu-32)/10} (1 - \beta)^2 (1 - \sqrt{2\alpha_0\beta^{\mu/2}})^{-6/5}. \quad (31)$$

## 4.2 Cooling time-scale

There are actually different approaches to calculate the cooling time-scale. We can estimate the cooling time-scale  $\tau_{\text{cool}}$

using simple cooling laws as the ratio of the internal energy density  $\epsilon = \Sigma c_s^2 / \gamma(\gamma - 1)$  to the cooling rate  $\Lambda$ , i.e.  $\tau_{\text{cool}} = \epsilon / \Lambda$ . Using equation (7), we can write

$$\Lambda = \left(\frac{1}{1-f}\right) \sigma T_{\text{eff}}^4 = \frac{3}{8\pi} \Omega_K^2 \dot{M} J(R). \quad (32)$$

On the other hand, angular momentum equation (6) gives

$$\alpha_0 H (p_{\text{gas}})^{\mu/2} p^{(2-\mu)/2} = \frac{3}{8\pi} \Omega_K \dot{M} J(R). \quad (33)$$

Having equation (33), we can rewrite equation (32) as

$$\Lambda = \alpha_0 H \Omega_K (p_{\text{gas}})^{\mu/2} p^{(2-\mu)/2}. \quad (34)$$

Thus, our cooling time-scale becomes

$$\tau_{\text{cool}} = \frac{1}{\alpha_0 \gamma (\gamma - 1)} \frac{1}{\Omega_K} \left(\frac{p_{\text{gas}}}{p}\right)^{(2-\mu)/2}, \quad (35)$$

and non-dimensional cooling time-scale becomes

$$t_{\text{cool}} = \frac{\tau_{\text{cool}}}{t_0} = \frac{1}{3\alpha_0 \gamma (\gamma - 1)} \beta^{(2-\mu)/2}, \quad (36)$$

where  $\gamma$  is the ratio of the specific heats and  $t_0 = 3/\Omega_K$ . According to Gammie (2001) and Lodato & Rice (2004) the fragmentation occurs when  $t_{\text{cool}} < 1$ .

## 4.3 Gravitational instability: A parameter study

When the disc cools very rapidly, the self-gravity of the disc does not have enough time to prevent the formation of bound objects in the disc. Since a corona extracts energy from the disc, we think, existence of the corona decreases the cooling time scale and the disc becomes more prone to fragmentation. As we have already mentioned, in the KS analysis of the gravitational instability of the disc and corona system, only the Toomre criteria has been used. Not only we consider this criterion of fragmentation, but the cooling time-scale condition is also considered in this paper.

Figure 4 shows the cooling time scale and the Toomre parameter versus radial location in the disc. For the energy exchange from the disc to the corona, the MN prescription is used and the other input parameters are  $\mu = 1.0$ ,  $\mu_m = 0.6$ ,  $\hat{\kappa} = 1$ ,  $\gamma = 2$  and  $M_8 = 1$ . Approximately, when  $\gamma = 5/3$  the cooling time-scale increases by a factor of two in comparison to the case with  $\gamma = 2$ . Each curve is labeled by a pair  $(\alpha_0, l_E/\epsilon)$ . Solid lines are for  $t_{\text{cool}}$  and dashed lines correspond to the parameter  $Q$ . In the inner parts of the disc, the Toomre parameter is very large, irrespective of the input parameters. Although the cooling time scale is less than unity (except for (0.03, 1)) in these regions, the Toomre condition for fragmentation does not satisfy and so the disc does not fragment. However, as we move toward larger radii, the Toomre parameter decreases down to the values smaller than unity. But the nondimensional cooling time-scale increases from small values at the inner parts of the disc to values greater or smaller than unity depending on the input parameters. Since in the MN prescription the amount of the transported energy from the disc to the corona is directly proportional to the viscosity coefficient  $\alpha_0$ , as this parameter increases, more energy is transported from the disc into the corona and the cooling time-scale decreases. According to Figure 4 when the viscosity coefficient is 0.03, the nondimensional cooling time-scale increases to values larger than

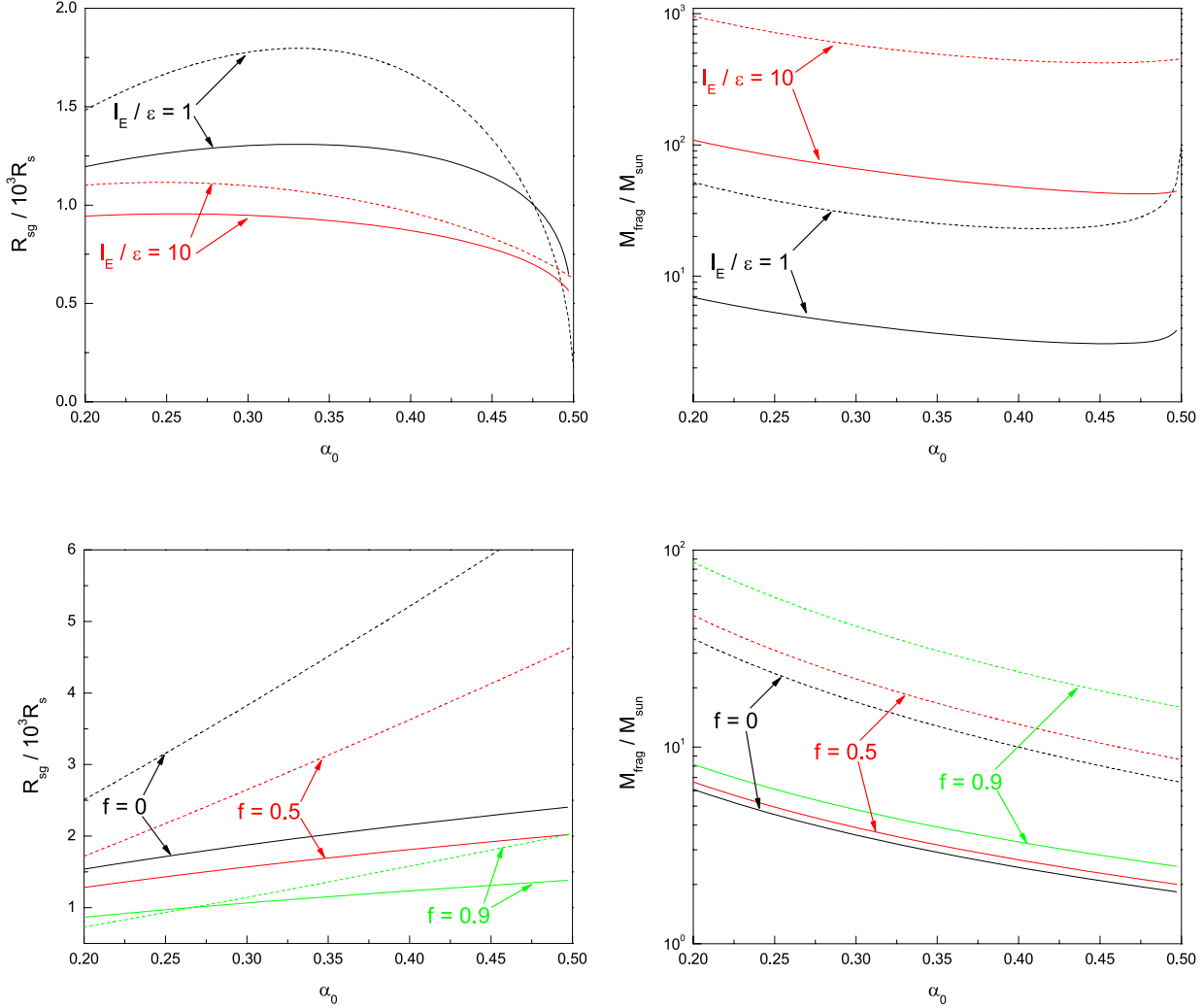


**Figure 6.** The self-gravitating radius  $R_{\text{sg}}$  (in Schwarzschild radius  $R_S$ ) and the mass of the first clumps  $M_{\text{frag}}$  (in solar mass) for  $\mu = 1.0$ ,  $\mu_m = 0.6$ ,  $\hat{k} = 1$ , and  $M_S = 1$ . *Top* plots are corresponding to the solutions with MN prescription and *bottom* plots are for the solutions with fraction  $f$  as a free parameter. Solutions with self-gravity are showing by solid curves, but dashed lines are corresponding to the solutions without self-gravity. For solutions with free  $f$ , each curve is labeled by this parameter and we assume  $l_E/\epsilon = 1$ .

unity at regions of the disc where the Toomre parameter is less than unity, irrespective of the accretion rate. When accretion rate decreases, the increase of  $t_{\text{cool}}$  becomes more smooth. However, for a larger viscosity coefficient 0.3 the cooling time-scale is lower than unity even at larger radii. So, in this case, the disc can fragment at regions where the Toomre parameter reaches to values lower than unity.

Figure 5 shows possible effects of the self-gravity of the disc on the Toomre parameter and the cooling time-scale. We compare curves of  $Q$  and  $t_{\text{cool}}$  for  $\alpha_0 = 0.03$  (top plot) and  $\alpha_0 = 0.3$  (bottom plot). While solid curves correspond

to our solutions, the dashed lines are for solutions neglecting the self-gravity of the disc (KS solutions). As we discussed, our solutions for  $\alpha_0 = 0.03$  are gravitationally stable considering cooling time-scale and Toomre conditions. However, we see that while the self-gravity of the disc slightly causes  $t_{\text{cool}}$  to decrease in the inner parts, this time-scale increases at larger radii. Even though  $Q$  is less than unity, since the dimensionless cooling time is long, the disc will not collapse complete but will be in a self-regulated self-gravitational state. Also, the effect of the self-gravity is more evident at high accretion rates. But for  $\alpha_0 = 0.3$  the cooling time-scale

is smaller than unity at all radii. Again, the self-gravity of the disc slightly causes the cooling time-scale to decrease in the inner parts, and a longer time-scale in the outer parts. So, when the Toomre parameter becomes less than unity, the disc becomes gravitationally unstable. In this case, the self-gravitating radius decreases because of the self-gravity of the disc, in particular at the high accretion rates.

Using equations (26) and (31) we can calculate the self-gravitating radius  $R_{\text{sg}}$  at which the Toomre parameter becomes unity and the mass of the fragments  $M_{\text{frag}}$  at this radius. Figure 6 shows results of the calculations for a system with a central mass of  $10^8 M_{\odot}$ , both for the solutions with MN prescription (top plots) and solutions with free fraction  $f$  (bottom plots). The other input parameters for the MN prescription are  $\mu = 1.0$ ,  $\mu_{\text{m}} = 0.6$ ,  $\hat{k} = 1$  and  $l_{\text{E}}/\epsilon = 1$  and 10. For comparison, while solid curves correspond to our solutions, the solutions neglecting self-gravity of the disc are shown by dashed curves. For the viscosity coefficient  $\alpha_0$ , we restrict to those values which correspond to a nondimensional cooling time-scale lower than unity. For values of the coefficient  $\alpha_0$  close to 0.5, the self-gravitating radius decreases. But the location of this radius is more sensitive to the viscosity coefficient for low accretion rates either with self-gravity or without it. Interestingly, the self-gravity of the disc causes the self-gravitating radius to decrease, in particular for low accretion rates. But as the viscosity coefficient increases, the self-gravitating radii of the solutions with self-gravity and without self-gravity become closer. On the other hand, we note that in the MN prescription the fraction of dissipated energy into corona is directly proportional to  $\alpha_0$ . Thus, as more energy is transported from the disc to the corona, the location of the self-gravitating radius becomes more independent of the self-gravity of the disc. Figure 6 (top; right plot) shows the mass of the fragments at the self-gravitating radius in the case of the MN prescription. The mass of the fragments increases significantly when the accretion rate is high and, generally, the mass of the fragments increases because of the existence of a corona (KS). But the self-gravitating radius decreases due to the existence of the corona either with low or high accretion rate. Consequently, the presence of a corona makes the disc more gravitationally unstable (KS). Also, the self-gravity of the disc significantly lead in reduction of the mass of the fragments for all values of the viscosity coefficient or accretion rate.

For comparison, the bottom plots of Figure 6 show the self-gravitating radius and the mass of the fragments for the solutions with free parameter  $f$ . Each curve is labeled by a corresponding fraction  $f$ . The other input parameters are  $\mu = 1.0$ ,  $\mu_{\text{m}} = 0.6$ ,  $\hat{k} = 1$  and  $l_{\text{E}}/\epsilon = 1$ . Again, solutions without self-gravity of the disc are shown by the dashed curves. For the effect of the self-gravity, in this case, behavior of the variations of  $R_{\text{sg}}$  and  $M_{\text{frag}}$  with the input parameter are qualitatively similar to the solutions with MN prescription: reduction of the self-gravitating radius due to the self-gravity of the disc, but as more energy is transported from the disc to the corona, location of the self-gravitating radius becomes independent of the self-gravity of the disc. However, the mass of the fragments significantly decreases due to the self-gravity of the disc, irrespective of the input parameters, notably the parameter  $f$ .

## 5 DISCUSSION

Generally and for simplicity, the radial or the vertical components of the gravitational force due to the self-gravity of the disc have been neglected in most of the analytical studies of self-gravitating accretion discs. However, some authors emphasize on the importance of the gravitational force due to the self-gravity of the disc (e.g., Paczynski 1978; Huré 1998; Bertin & Lodato 1999). To our knowledge, most of the previous studies of star formation in AGNs or the Galactic center do not consider the components of the gravitational force due to the self-gravity of the disc (e.g., Goodman & Tan 2004; Nayakshin & Cuadra 2005). Although KS studied the possible effects of a corona on the gravitational stability of an accretion disc, they also neglected the components of the self-gravity of the disc itself. In this work, we presented sets of analytical solutions for the steady-state structure of self-gravitating accretion discs with corona. We also considered the vertical component of the gravitational force due to the self-gravity of the disc. The energy exchange between the disc and the corona has been considered either as a function of the physical variables of the disc, or as a free parameter of the model. Although there are possible mass and angular momentum exchanges between the disc and the corona, we have neglected these effects just for simplicity in order to present a self-consistent model for a disc-corona system. Having the analytical solutions, we studied properties of the solutions, more importantly gravitational stability of the disc. For the conditions of fragmentation, not only the Toomre parameter but the cooling time-scale are considered in our analysis.

We showed that because of the energy exchange, the corona lead in a cooler the disc for all the input parameters. This reduction of the temperature due to existence of the corona, decreases the thickness of the disc. Since there is no mass exchange between the disc and corona, the surface density increases and as a result, the vertical component of the gravitational force due to the self-gravity of the disc becomes more effective. When the Toomre parameter reaches to around unity, the ratio  $\zeta$  is around 4.8 which means that the vertical component of the gravitational force due to the self-gravity of the disc is a few times larger than the vertical component of the gravitational force of the central object at the self-gravitating radius. Thus, this term may modify properties of the solutions as our solutions show. For example, self-gravity of the disc in a disc-corona system causes the surface density to decrease at the inner parts of the disc, though the temperature of the disc is unchanged when the self-gravity of the disc is considered.

Considering Toomre parameter and cooling time-scale conditions for fragmentation, solutions with small viscosity coefficients are stable to fragmentation because in the inner parts of the disc  $Q \gg 1$  and when Toomre parameter reaches to unity, the cooling time-scale becomes greater than one. This result is independent of the accretion rate or other input parameters. But for large viscosity coefficient the cooling-time scale is smaller than one for all radii, and so, once the Toomre parameter becomes less than one the disc may fragment. However, the cooling time-scale slightly decreases at the inner parts of the disc because of the self-

gravity of the disc and for high accretion rates, this time-scale increases.

Also, self-gravitating radius and the mass of the fragments at self-gravitating radius decrease because of the self-gravity of the disc. However, change of the self-gravitating radius due to the self-gravity is negligible when the amount of the energy which is transported from the disc to the corona is increased. But reduction of the mass of the fragments because of the self-gravity is independent of the fraction  $f$ . These results are obtained either with free  $f$  or MN prescription for the fraction of energy exchange. Although we estimate the mass of the fragments in an accretion disc with corona around supermassive blackholes, we can not determine whether these fragments are sufficiently long-lived to be able to evolve in protostars over many orbital periods.

## ACKNOWLEDGMENTS

We thank an anonymous referee for very useful suggestions which have significantly improved the paper. FK acknowledges the support of an Ad Astra PhD Scholarship from University College Dublin. PD is grateful to the Dublin Institute for Advanced Studies where part of this research was carried out. We thank Cliona Golden for reading the paper and her useful comments.

## REFERENCES

- Bertin G., Lodato G., 1999, *A&A*, 350, 694  
 Bertout C., *ARA&A*, 1989, 27, 351  
 Blackman E. C., Field G. B., 2000, *MNRAS*, 318, 724  
 Czerny B., 2007, *ASPC*, 360, 265  
 Cannizzo J. K., Reiff C. M., 1992, *ApJ*, 385, 87  
 Galeev A. A., Rosner R., Vaiana G. S., 1979, *ApJ*, 229, 318  
 Gammie C. F., 2001, *ApJ*, 553, 174  
 Goodman J., 2003, *MNRAS*, 339, 937  
 Goodman J., Tan J. C., 2004, *ApJ*, 608, 108  
 Fukue J., Sakamoto C., 1992, *PASJ*, 44, 553  
 Haardt F., Maraschi L., 1991, *ApJ*, 380, L51  
 Hunter J. H., Ball R., Gottesman S. T., 1984, *MNRAS*, 208, 1  
 Huré J. M., Collin-Souffrin S., Le Bourlot J., Pineau des Forêts G., 1994, *A&A*, 290, 19  
 Huré J. M., 1998, *A&A*, 337, 625  
 Lodato G., Rice W. K. M., 2004, *MNRAS*, 351, 630  
 Lu Y., Yang L., Wu S., *A&A*, 327, 57L  
 Karas V., Huré J. M., Semerák O., 2004, *Class. Quantum Grav.*, 21, R1  
 Kawaguchi T., Shimura T. & Mineshige S., 2001, *ApJ*, 546, 966  
 Khajenabi F., Shadmehri M., 2007, *MNRAS*, 377, 1689 (KS)  
 Köhler R., 1995, *A&A*, 294, 690  
 Kozłowski M., Wiita P. G., Paczyński B., 1979, *AcA*, 29, 157  
 Kuncic Z., Bicknell G. V., 2004, *ApJ*, 616, 669  
 Liang E. P. T., Price R. H., 1977, *ApJ*, 218, 247  
 Mejia A. C., Durisen R. H., Pickett M. K., Cai K., 2005, *ApJ*, 619, 1098  
 Merloni A., Fabian A. C., 2001a, *MNRAS*, 328, 958  
 Merloni A., Fabian A. C., 2001b, *MNRAS*, 321, 549  
 Merloni A., Nayakshin S., 2006, *MNRAS*, 372, 728  
 Nayakshin S., Cuadra J., 2005, *A&A*, 437, 437  
 Osterbrock D.E., 1993, *ApJ*, 404, 551  
 Paczyński B., 1978, *AcA*, 28, 91  
 Rice W. K. M., Lodato G., Armitage P. J., 2005, *MNRAS*, 364, L56  
 Rice W. K. M., Armitage P. J., Bate M. R., Bonnell I. A., 2003, *MNRAS*, 339, 1025  
 Robinson J., 1976, *ARA&A*, 19, 119  
 Sakimoto P. J., Coroniti F. V., 1981, *ApJ*, 274, 19  
 Shields G., 1978, *Nature*, 272, 706  
 Shore S. N., White R. L., 1982, *ApJ*, 256, 390  
 Svensson R., Zdziarski A. A., 1994, *ApJ*, 436, 599  
 Szuszkiewicz E., 2001, *MmSAI*, 72, 65  
 Toomre A., 1964, *APJ*, 139, 1217  
 Taam R. E., Lin D. N. C., 1984, *APJ*, 287, 761  
 Watarai K. Y., Mineshige S., 2003, *APJ*, 596, 421  
 Wang J-M., Watarai K-Y., Mineshige S., 2004, *ApJ*, 607, 107  
 Yang L. T., Liu X. C., 1990, *ApSS*, 172, 293